Additive manufacturing of a high strength Al-5Mg_2Si-2Mg alloy: microstructure and mechanical properties

Hailin Yang[1]*, Yingying Zhang[1], Jianying Wang[1], Zhilin Liu[2], Chunhui Liu[2], Shouxun Ji[3*]

1. State Key Laboratory of Powder Metallurgy, Central South University, Changsha 410083, China

2. Light Alloy Research Institute, College of Mechanical and Electrical Engineering, Central South University, Changsha, 410083, P.R. China

3. BCAST, Brunel University London, Uxbridge, Middlesex, UB8 3PH, United Kingdom

*Corresponding authors: Hailin Yang, y-hailin@csu.edu.cn; Shouxun Ji, shouxun.ji@brunel.ac.uk

Abstract

A novel Al-5Mg_2Si-2Mg alloy was processed by selective laser melting (SLM) to understand its representative features of microstructural evolution and mechanical properties during additive manufacturing (AM). The as-SLM fabricated Al-5Mg_2Si-2Mg alloy is found to deliver much less hot cracks and other defects. Meanwhile, excellent mechanical property is also achieved, i.e. 452±11 MPa for ultimate tensile strength, 295±14 MPa for yield strength, and 9.3±2.5% for elongation. Clearly, these mechanical properties are better than that obtained by high pressure die casting (HPDC), and better than some other alloys obtained by SLM. The as-SLM fabricated Al-5Mg_2Si-2Mg alloy is featured by the significantly refined microstructures in the compact primary α-Al, the divorced Mg_2Si eutectic networks distributing at α-Al grain boundaries, and some α-AlFeMnSi phase in association with eutectic Mg_2Si phase. The high strength and ductility of the alloy is attributed to its unique features including (a) the reduced solidification range, (b) the possible increase of the eutectic level in the microstructure, and (c) the shift of eutectic point and the maximum solubility point of Mg_2Si in Al matrix.

Key words: Aluminium alloys; Additive manufacturing; Selective laser melting; Microstructure; Mechanical properties.

1. Introduction

Selective laser melting (SLM) has been attracting significant attention in manufacturing net shape components with industrial scale products because of its promising capability of fabricating complex geometries directly from computer-aided design (CAD) models [1,2]. In addition to the improvement of design flexibility and cost reduction, SLM can also deliver equivalent or even improved mechanical properties compared to cast and/or wrought counterparts in Ti alloys, Ni-based superalloys, and stainless steel, etc. However, the fabrication of high-performance aluminium alloys using SLM is much more challenging because aluminium alloy powders usually have poor flowability, high laser reflectivity and high thermal conductivity, resulting in a demand of high laser power to overcome the rapid heat dissipation [2,3]. Moreover, aluminium alloys are highly prone to oxidation and easy to form porosity and other defects [4,5]. Therefore, the mechanical properties of common aluminum alloys fabricated by SLM are far from satisfaction and special cares are necessary for SLM of aluminium alloys.

In SLM fabricated aluminium alloys, both wrought alloys and cast alloys have been considerably studied for the commercially available alloys. However, it is found that SLM fabricated Al-Si based alloys [6] can offer good strength with low defects, but poor ductility under as-built condition. The SLM fabricated Al-Cu based [7,8], and/or Al-Zn-Mg-Cu based alloys [9] can provide high strength but high susceptibility of hot cracking. Also, the Al-Mg-Sc-Zr based alloys [10,11] are high cost, although the strength and elongation are very good. Therefore, it becomes important to develop a new SLM fabricated Al alloy that have good strength, good ductility, low hot-crack susceptibility and low cost. In the meantime, some SLM fabricated aluminium alloys were thermally treated through solution and/or ageing in order to achieve higher strength. However, high temperature solution introduces high residual stress and easy to cause distortion in industrial components. Also, the heat treatment itself consumes energy. More importantly, the existing results showed that many solution and ageing heat treatment processes are not beneficial for mechanical properties of SLM fabricated aluminium alloys because of the introduction of casting defects [12,13,14]. Therefore, it is more attractive to have improved mechanical properties in the SLM fabricated parts without or with minimal heat treatment.

In principle, most engineering AlSiMg and AlMgSi alloys are Al-Mg_2Si based materials. These can be expressed as Al-Mg_2Si alloys with extra Si and/or Al-Mg_2Si

alloys with extra Mg. Most of the commercially available wrought alloys and cast alloys are Al-Mg_2Si with extra Si. These alloys can be solutionised and/or aged for improving the mechanical properties by forming precipitates during heat treatment. The studied alloys of AA6061, A5052, A5083 and Al10SiMg (Silafont 36) are fallen to this category. However, there is limited study for the alloys belonging to Al-Mg_2Si with extra Mg, from which the microstructure and mechanical properties are all unclear for the SLM fabricated materials. On the other hand, the research in high pressure die casting (HPDC) have confirmed that, under as-cast condition, some Al-Mg_2Si alloys with extra Mg can offer better mechanical properties than many Al-Mg_2Si alloys with extra Si [15,16,17]. Therefore, it is attractive to study the Al-Mg_2Si alloys with extra Mg using SLM process to improve the mechanical properties under as-SLM fabricated condition.

In the present paper, we aim to study the microstructure and mechanical properties of Al-5Mg_2Si-2Mg alloy, in which the characterization of powders, microstructure, phase formation and tensile properties were investigated. The discussion focuses on the microstructural evolution, the mechanical properties and the associated strengthening mechanisms.

2 Materials and methods

2.1 Pre-alloyed powder preparation

Al-5Mg_2Si-2Mg alloy powders were manufactured in house by gas atomization. High purity argon was selected as protective atmosphere to avoid the oxidization during atomization. The chemical composition of raw pre-alloyed powder was calibrated by inductively coupled plasma atomic emission spectrometry (ICP-AES) and the results are listed in Table 1. The alloy powder was sieved into a size distribution range of 7-50 μm and the mean size of 25.9 μm, which was measured using a laser particle size analyzer (Matersizer). The details for the particles are shown in Figure 1. The powder exhibited spherical shape with a slight satellite ball particle (Figure 1a). It is also seen from Figure1(c) and (d) that few flaws were observed in the cross-section of the powder. The primary α-Al phase in Figure 1d showed dendritic liked shape with a size of ~10 μm. The very fine eutectic Mg_2Si phase was distributed between the α-Al phases.

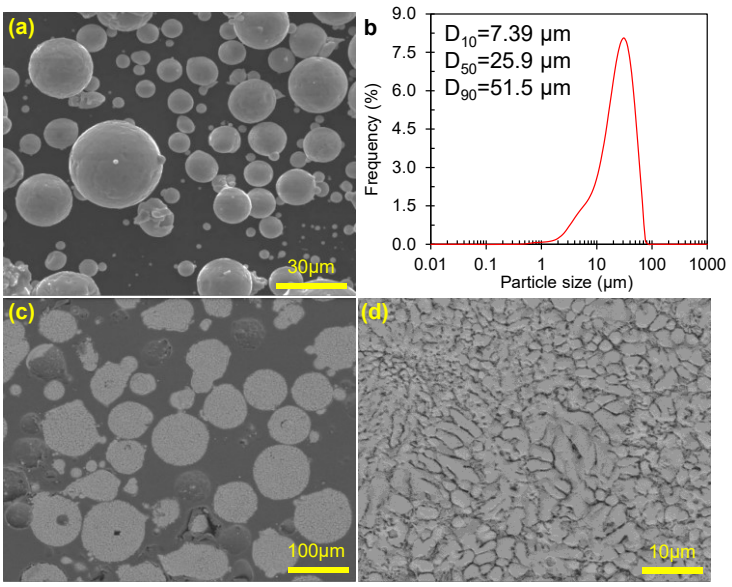

Figure 1 (a) SEM image showing the morphology of Al-5Mg_2Si-2Mg alloy powder with Ar gas atomization; (b) Particle size distribution of the atomized powder; (c) and (d) SEM images showing the morphology of atomized article on the cross section and detailed microstructure of Al-5Mg_2Si-2Mg alloy.

Table 1 The composition of experimental alloy powder calibrated by ICP-AES (in wt.%).

Alloy		Mg	Si	Mg_2Si	Mn	Fe	Others	Al
Al-5Mg_2Si-2Mg	wt.%	2.03	-	5.05	0.42	0.11	<0.08	Bal.

2.2. SLM fabrication process

A FS271M SLM system (Farsoon, Inc, China) were utilized to fabricate alloy samples. The SLM machine was equipped with a 500 W Gaussian beam fiber laser with a focal laser beam diameter of 90 μm. The SLM operation was performed in an inert argon atmosphere to avoid oxidation of the alloy. The samples were built layer-by-layer on an aluminum alloy plate of 6061, which was grit-blasted with alumina prior to installation. The laser scanning strategy was used 67° rotating scanning layer-by-layer.

The cubic samples with the dimension of 10×10×10 mm were initially printed using different processing parameters. Processing parameters were set as follows: hatch spacing (h) at 0.1 mm, layer thickness (t) at 0.05 mm, laser power (P) at 270, 310, 350, 390, and 430 W, scan speed (v) at 500, 800, 1000, 1200, and 1400 mm·s^{-1}. The calculated laser energy density-range are VED=54 J·mm^{-3} to VED=125 J·mm^{-3}

according to Eq. (1) [18,19].

$$VED = \frac{\mathrm{P}}{\mathrm{d}\cdot\mathrm{t}\cdot V_s} \quad (1)$$

where P is the laser power (W), V the scan speed (mm/s), h the hatching space (mm), and t the layer thickness (mm). According to Eq. (1), a high laser energy density can be obtained by increasing the laser power, and/or decreasing the layer thickness or the hatching space. The dog-bone-shaped tensile samples with a gauge length of 25 mm and cross-section 4.0 × 2.0 mm^2 were printed based on the optimal printing parameters. The as-printed samples were then machined into one batch in order to maintain the similar levels of machining errors.

2.3. Characterization

The relative density of the SLM processed samples was measured by Archimedes Drainage Method. Phase constituents were identified using X-ray diffraction (XRD) from a Rigaku X-2000 diffractometer with Cu Kα radiation (λkα = 1.54 Å) at 40 kV. The samples were mechanically polished and etched using Keller's solution for SEM examination. The microstructures were observed using an FEI nano 230 field emission scanning election microscope (FE-SEM) equipped with an energy dispersive X-ray spectrometer (EDS). The grain size and preferred lattice were measured at microscale using electron backscattered diffraction (EBSD) in a different SEM (Hitachi S-3400 N). EBSD was equipped with an Oxford instrument Aztec HKL® imaging system. To distinguish the detailed microstructure, further characterizations were performed using transmission electron microscope (TEM: Tecnai G2 F20) operated at 200 kV. Thin foil specimens for the TEM analysis were prepared using focusing ion beam (FIB).

2.4 Mechanical properties

Dog-bone-shaped tensile samples were cut by electrical discharge machining from the printed samples. Both sides of the specimens were carefully ground to a 2000 grit finish using a SiC paper. The uniaxial tensile tests were performed using a material testing system (MTS Alliance RT30) at room temperature (≈20 °C) with an engineering strain rate of 1×10^{-3} s^{-1}. Micro-hardness was measured by a

micro-Vickers hardness tester with a load of 300 g for 10 s (ASTM E 384-08). All the reported data are the average value of at least 5 measurements.

3. Results

3.1 SLM fabrication processing windows

Figure 2 shows the variation of relative density with the applied volumetric energy density (VED) for the cube samples. It is seen that the relative density had a rapid increase up to 99.5% with increasing the VED up to 77.5 J·mm^{-3}, followed by a plateau at the mean relative density of 99.5 ± 0.07% when the VED ≥ 77.5 J·mm^{-3}. Clearly, the further increase in the VED was not significant to maximize the density of printed samples in our experimental. Therefore, the VED ≥77.5 J·mm^{-3} should be a good option for achieving the material density ≥99.5%. The dependence of material density ρ on VED shown in Figure 2 can be described by a mechanical growth model according to Eq. (2):

$$\rho = c_1(1 - c_2 \cdot 10^{-c_3 \cdot VED}) \qquad (2)$$

The fitted parameters using the Euler-method are c_1=0.996±0.0003, c_2=0.283±0.109 and c_3=0.0497±0.006.

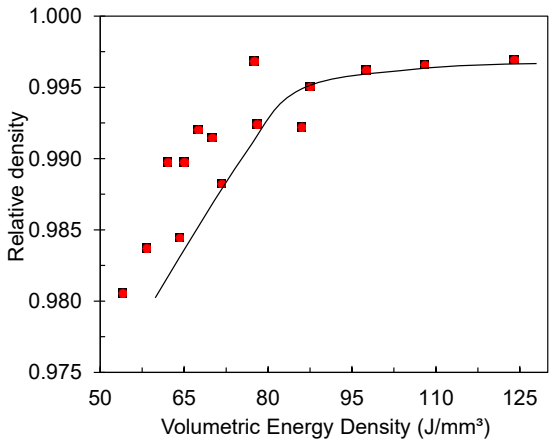

Figure 2 The relationship between relative density and volumetric energy density.

In the meantime, the increase of scanning speed led to a linear decrease of VED. The laser power was also proportional to the VED. Therefore, the selection of scanning speed and laser power in SLM process should be based on the VED. The effect of VED on the hardness of as-SLM fabricated Al-5Mg$_2$Si-2Mg alloys is shown in Figure 3. With increasing the VED, the micro-harnesses showed a slight increase and then a

slight decrease. The peak hardness was at 80 J/mm^3 VED. Previous studies have shown that the hardness can be tailored by changing processing parameters [20, 21, 22]. At lower VEDs, the presence of undissolved alloy particles due to lack of fusion, and the balling effect could result in lower hardness. However, as the VEDs are relatively high, numerous melt pools and splashes from inside the unstable melt pools lead to severe gas inclusions in the melt, which ultimately deteriorates the hardness. Additionally, it is observed that the micro-harnesses were higher in the horizontal direction than those in the building direction. Based on the sample density and hardness, the optimized processing parameters were defined as: Vs= 800 mm/s, and P=310 W, VED= 80 J/mm^3.

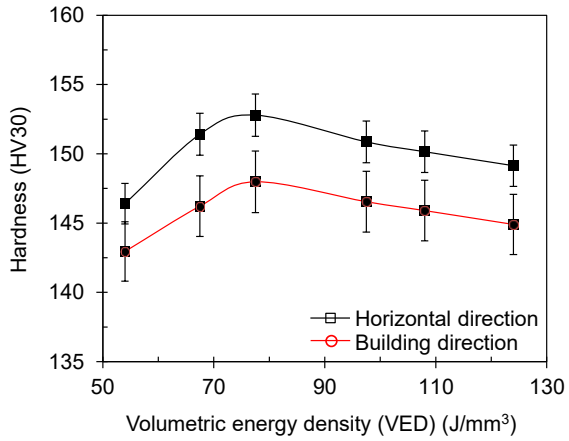

Figure 3 The effect of volumetric energy density on the hardness of as-SLM fabricated Al-5Mg_2Si-2Mg alloy.

3.2 Phase analysis

Figure 4 shows the XRD spectra of Al-5Mg_2Si-2Mg alloy under powder and as-SLM fabricated condition. It is obvious that the diffraction of α-Al and Mg_2Si peaks was clearly visible in the powder and SLM fabricated samples. No new phase was introduced during SLM processing. It is also noted that the peaks of Mg_2Si were weakened for the SLM fabricated samples, indicating that some Mg_2Si phase was possibly solutionised into α-Al matrix due to the high heating/cooling rate during SLM fabricating process.

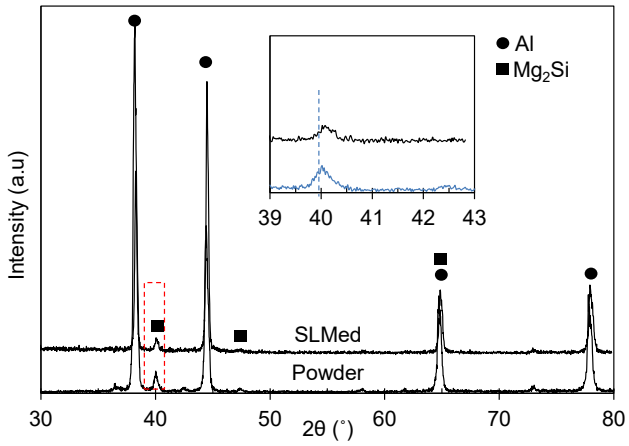

Figure 4 XRD spectra of the experimental alloy under powder and fabricated conditions.

3.3 Refinement in as-fabricated microstructure

Figure 5 shows the EBSD image of as-SLM fabricated alloy along horizontal direction and building direction, which are parallel and perpendicular to the base plate, respectively. It can be observed that the individual grain on the matrix with different colors. The microstructure on the cross plane parallel to the base plate consisted mostly of equiaxed grains at an average size of 20 μm with very fine of 1 μm in the local area. Along the vertical direction on the cross-plane perpendicular to the base plate, the morphology of columnar grains is obvious and the size can be up to hundreds of microns long and up to 1-20 μm wide. Moreover, it is noted that some regions in the conjunction areas of the columnar grains contained fine equiaxed grains. It is also seen that no significant texture evolutions were obtained in the as-fabricated microstructure. Similar results have been observed in the as-SLM fabricated other aluminium alloys [2,5].

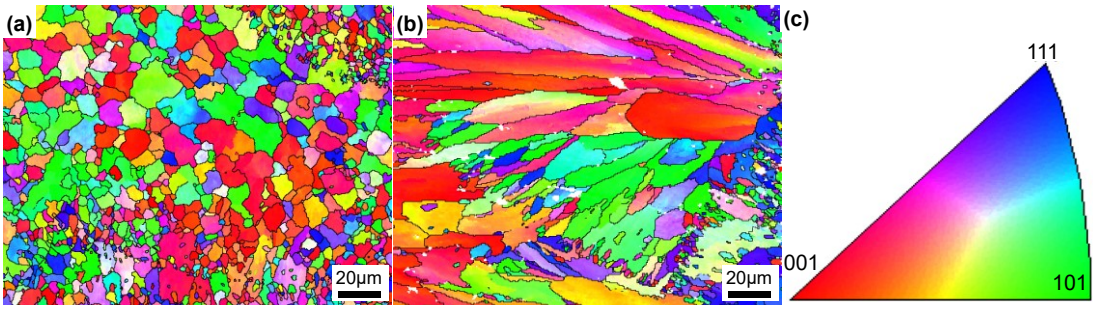

Figure 5 EBSD images of as-fabricated Al-5Mg_2Si-2Mg alloy along (a) the horizontal direction (in cross plane parallel to base plate), (b) the building direction (in cross plane perpendicular to base plate), and (c) corresponding IPF map.

To further understand the detailed characteristics of as-SLM fabricated microstructure, Figure 6 shows the detailed microstructure along the horizontal direction (Figure 6a-c) and along the building direction (Figure 6d-f). The typical microstructure was controlled by melt pool (MP). It is seen a MP coarse zone observable in the matrix in both directions. In the horizontal direction, the equiaxed grains contain a homogenously distributing cell-like sub-structure typically on the scale of about 500 nm, with boundaries of Mg_2Si rich-regions. The typical feature in the horizontal direction is that the equiaxed grains existed in the whole section, only difference was the tiny fine grains in the edge of MP zone. However, in the building direction, three zones were clearly observed in the microstructure. A heat affected zone (HAZ) was seen as a transition between MP coarse and MP fine zones. Two differences were found in the microstructures: (1) the equiaxed grain is much large in the building direction (Figure 6e) was much coarser than that in the horizontal direction (Figure 6b); (2) the columnar grains along the vertical direction contained a homogenously distributing nano fiber-like structure, as indicated in Figure 6f. These suggest that the effect of base plate heating is obvious. Clearly, no dendritic microstructures were observed in the as-SLM fabricated Al-5Mg_2Si-Mg alloy, but the coarsened equiaxed grains were found. The typical lamellar eutectic structures were also not observed, but the fiber-like structure should be the eutectic structure under as-SLM fabricated condition. Measurements of the volume fraction of Mg_2Si eutectic have been carried out on the secondary electron images obtained in SEM. These measurements confirmed that there was about 30.63±0.05 vol.% in the MP fine zone and 24.26±0.03 vol.% in the MP coarse zone of Mg_2Si in cells, sub cells and grain boundaries in the as-fabricated samples. Another feature in the microstructure was that the refined microstructure was actually not uniformed, the local heterogeneity was clearly the results of multistage solidification in the melt pools.

To further confirm the element distribution in the refined microstructure, HAADF-STEM image and the elemental mapping of cell-like sub-structure are shown in Figure 7. It is seen that the Mg and Si distributed clearly along the Al grain boundaries, confirming the Al-Mg_2Si eutectics were formed in a divorced approach and showed no traditional lamellae structure in the eutectic cell. It is also noted that Mn and Fe were precipitated together with Mg_2Si. The morphological features showed likely as α-AlFeMnSi phase. The detailed HAADF-STEM image and the elemental mapping of Fe-rich phase are present in Figure 8. It is confirmed that the

Fe-rich phase is composed of Al, Fe, Mn, and Si. Therefore, although the exact composition was not able to measure in the fine structure, the morphological feature and component elements indicated the Fe-rich intermetallics is most likely to be the same one found in die casting process [23].

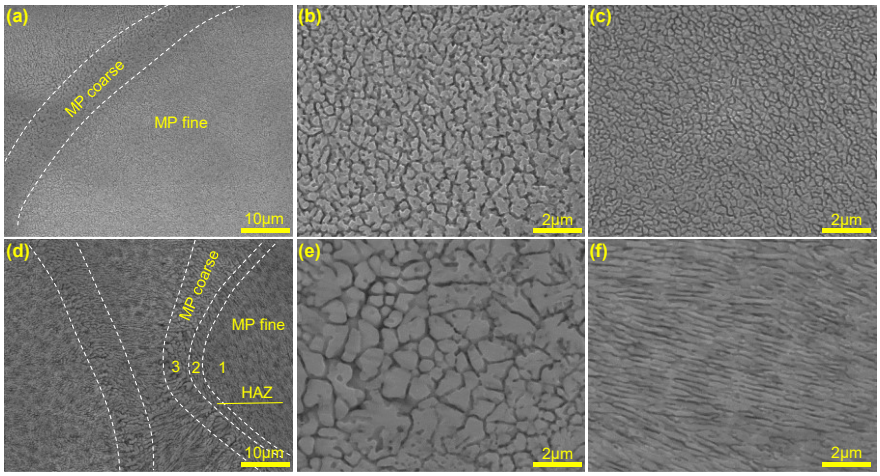

Figure 6 SEM images showing (a) the overall microstructure, (b) the detailed microstructure in zone 3, and (c) the detailed microstructure in zone 1 along the horizontal direction; (d) the overall microstructure, (e) the detailed microstructure in zone 3, and (f) the detailed microstructure in zone 1 along the building direction in the SLM fabricated Al-5Mg_2Si-2Mg alloy. 1- MP fine zone, 2- HAZ (heat affected zone), 3- MP coarse zone.

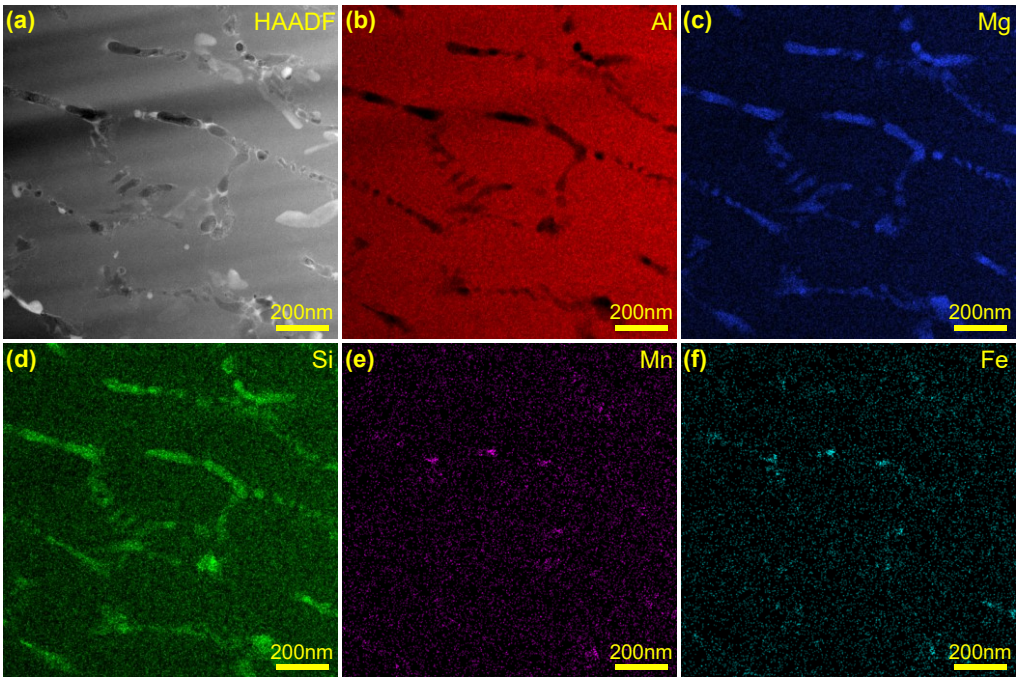

Figure 7 HAADF-STEM image showing the microstructures of as-built Al-5Mg_2Si-2Mg alloy and individual elemental mapping of Al, Mg, Si, Mn and Fe.

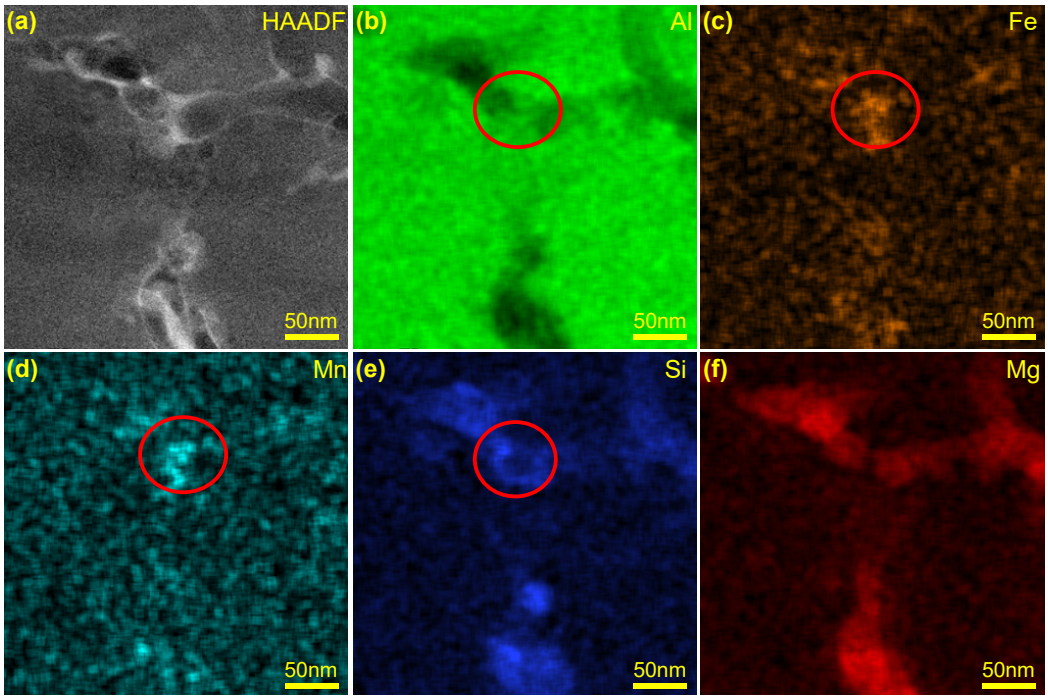

Figure 8 HAADF-STEM image showing the microstructures of intermetallic phase in the as-built Al-5Mg_2Si-2Mg alloy and individual elemental mapping of Al, Fe, Mn, Si and Mg.

Figure 9 shows the detailed microstructure in the cellar structure and the interface of Al/Mg_2Si with the orientation of FTT. It can be seen that the cell-like sub-structure were identified as Al cells and the Mg_2Si was distributed around the individual Al cell. Critically importantly, the HR-TEM in Figure 9b showed the interface of Al/Mg_2Si had a good orientation with $(001)_{Al}//(001)_{Mg2Si}$. The atoms could be coherent each other at the interface. This is critical for strengthening mechanism as a coherent interface means that a precipitation strengthening is possibly developed under certain condition, which will be possibly open a window for SLM processing.

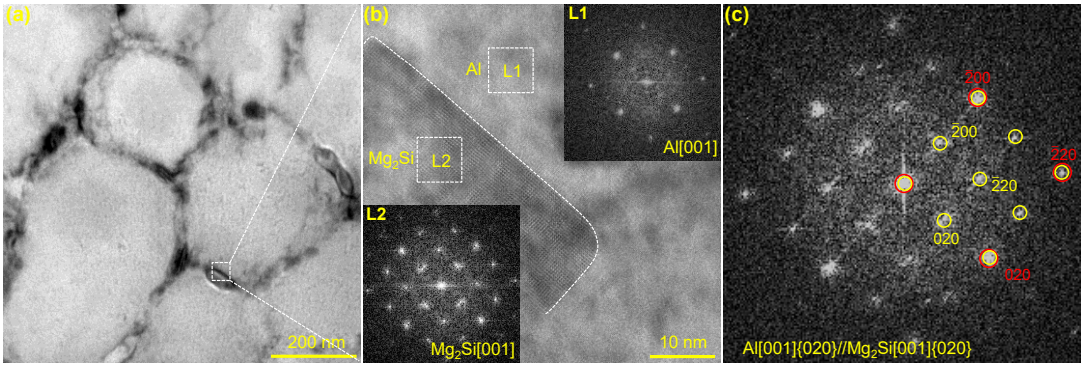

Figure 9 (a) Bright field TEM showing the detailed microstructure in the cellar structure and (b) and (c) HRTEM showing the interface of Al/Mg_2Si and the inserts showing the orientation of FTT.

3.3 Mechanical properties

Figure 10 shows the tensile strength–strain curves of as-SLM fabricated Al-5Mg_2Si-2Mg alloy. It is seen that the as-SLM fabricated Al-5Mg_2Si-2Mg alloy offered excellent mechanical properties, including the ultimate tensile strength (UTS) of 452±11 MPa, the yield strength of 295±14 MPa and the elongation of 9.3±2.5%. The tested samples exhibited a good consistence in the yield strength, UTS and elongation because of the very small difference in the tensile properties.

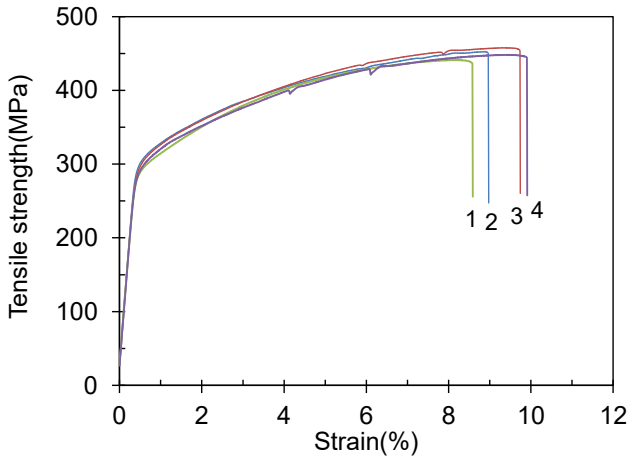

Figure 10 Tensile stress-strain curves of as-SLM fabricated Al-5Mg_2Si-2Mg alloy.

In order to understand the properties offered by different aluminium alloys processed by SLM. Table 2 listed the detailed comparisons in the yield strength, UTS and elongation from published data. It is seen that, as the popular hypoeutectic aluminum alloy, Al-(7-10)Si-Mg have been tried by different researchers. However, the yield strength, UTS and elongation were very different in the results obtained by different researchers, in which the UTS was from 284 to 434 MPa, the yield strength was from 182 to 322 MPa and the elongation was from 1 to 25 %. Clearly, the UTS, yield strength and elongation of as-SLM fabricated Al-5Mg_2Si-2Mg alloy were much higher than that of most of the as-SLM fabricated Al-Si-Mg alloys. More precisely, as the first data reported for Al-5Mg_2Si-2Mg alloy processed by SLM, the results showed an excellent combination of strength and ductility. It is noted that the solution treatment and ageing heat treatment of Al-(7-10)Si-Mg alloys are not very beneficial for the property improvement as the inherent gas contents is high in SLM fabricated alloys.

Table 2 Mechanical properties of SLM fabricated Al-Si alloys from different literatures

Material	Condition	Yield strength (MPa)	UTS (MPa)	Elongation (%)	Ref.
Al-5Mg_2Si-2Mg	As-SLM fabricated	295±14	452±11	9.3±2.5%	This work
Al7Si0.3Mg	As-SLM fabricated horizontal	210	400	11	[24]
	As-SLM fabricated vertical	200	390	10	[24]
Al7Si0.6Mg	As-SLM fabricated horizontal	280	410	7.5	[25]
	As-SLM fabricated vertical	240	400	7	[25]
Al9Si3Cu	As-SLM fabricated	219±20	374 ± 11	1.9 ± 0.2	[26]
	As-SLM fabricated	236±8	415 ± 15	5.0 ± 2.0	[27]
Al10SiMg	As-SLM fabricated horizontal	245	~330	1.2	[28]
	As-SLM fabricated vertical	220	310	1	[28]
	As-SLM fabricated	–	396	3.5	[29]
	As-SLM fabricated		360	6	[30]
	As-SLM fabricated	268+2	333+15	1.4+0.3	[31]
	As-SLM fabricated	255±13	377±13	2.2±0.2	[32]
	As-SLM fabricated horizontal	182	282	25	[33]
	As-SLM fabricated vertical	184	284	18	[33]
	As-SLM fabricated horizontal	206-241	360-390	5-6	[33]
	As-SLM fabricated vertical	198-208	345-357	3	[34]
Al11SiCuMn	As-SLM fabricated	350 ± 5	470 ± 18	1.8 ± 0.4	[34]
Al12Si	As-SLM fabricated	225	360	5	[36]
	As-SLM fabricated	260 ±5	380	3	[37]
Al12Si0.75Mg	As-SLM fabricated	354.9	427.7	2.54	[38]

Similarly, the yield strength, UTS and elongation obtained from SLM fabricated Al-5Mg_2Si-2Mg alloy were all higher than that of Al-Si-Cu and Al-Si alloy. However, the as-SLM fabricated Al-5Mg_2Si-2Mg alloy offered less yield strength, UTS and elongation than AlZnMg alloys and AlMnScZr alloys. Overall, the resultant mechanical property confirmed that the Al-5Mg_2Si-2Mg alloy can be proceed by SLM and can offer excellent combination of yield strength, UTS and elongation, which is applicable in industry under as-fabricated condition.

4. Discussion

4.1. Alloy features and microstructural evolution

Al-Mg_2Si based alloys are important in casting materials. The main advantages come from the unique features of magnesium silicide (Mg_2Si), which exhibits low density (1.99×10^3 kg·m^{-3}), high melting temperature (1085 °C), high hardness (4.5×10^9 N·m^{-2}), high elastic modulus (120 GPa) and low coefficient of thermal expansion (7.5×10^{-6} K^{-1}). Moreover, Mg_2Si benefits castability in aluminium alloys. Therefore, Al-Mg_2Si based alloys show excellent combination of physical and mechanical properties.

Generally, binary Al-Mg_2Si alloy actually represents a ternary system with a ratio of 1.73 between Mg and Si. Al-Si-Mg alloy with this specific Mg:Si ratio is able to be further strengthened by precipitate strengthening with solution and ageing process. In our studies, it is found the addition of extra Mg into Al-Mg_2Si alloy can shift the eutectic point and the maximum solubility point of Mg_2Si in Al to the left, as shown in Figure 11a. Therefore, the Al-Mg_2Si-Mg alloy can offer a few unique advantages including (1) the reduced solidification range with the same amount of Si, which is beneficial for the reduction of shrinkage during solidification. (2) the possible increase of the eutectic level in the microstructure. Theoretically, through maintaining the same amount of Si in the alloy, the addition of Mg could make the alloy as a eutectic alloy. Therefore, the strengthening from secondary phase is possibly enhanced. (3) The shift of the maximum solubility points of Mg_2Si in Al matrix results in the malfunction of precipitate strengthening through solution and ageing process. More importantly, these will result in the improvement of castability because of the decrease of solidification range and existence of Mg_2Si, which can significantly reduce the casting defects. Therefore, the much-improved elongation can be obtained as shown in Figure 10, which clearly showed the ductility (9% elongation) of studied alloy is much higher than most of SLM Al-Si alloys (1~5% elongation) under as-fabricated condition.

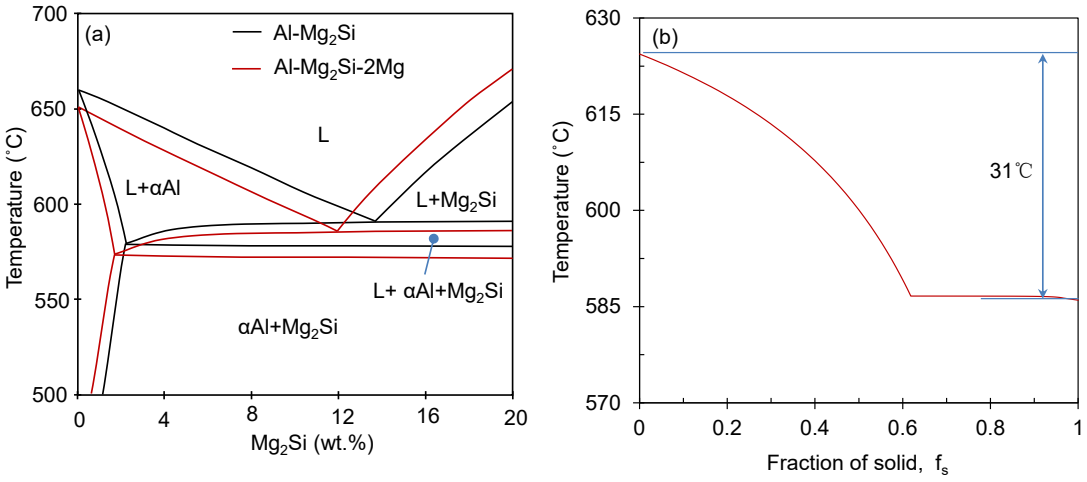

Figure 11 (a) Equilibrium phase diagram of Al-Mg_2Si and Al-Mg_2Si-2Mg alloys calculated by Pandat, and (b) the fraction of solid phase evolved during solidification calculated using Scheil-Gulliver non-equilibrium solidification model for Al-5Mg-2Si alloy.

The hot cracking susceptibility can be qualified using the hot cracking index developed by Easton et al. [39] as $CSI_E = \int_{T_0}^{T_{co}} f_s \, dT$ and another version developed by Kou [40,41] as $CSI_K = \max \left| \frac{dT}{d\sqrt{f_s}} \right| \; for \; f_s \leq f_{s,co}$ where T is temperature and f_S the fraction solid in the semisolid. The index is closely linked to the steepness of the solidification curve near $(f_S)^{1/2}$=1. An alloy exhibiting a greater steepness tends to be more susceptible to cracking during solidification. Therefore, the hot-crack-susceptible alloys can be identified from their solidification curves. The shapes of these curves are determined by the compositions of the constituent alloys and can be described using a Scheil-Gulliver solidification model based on the equilibrium phase diagram, as shown in Figure 11b for Al-5Mg_2Si-2Mg alloy. Pandat was used to simulate sequential steps from the liquidus temperature to an approximate solidus temperature through the calculation of the fraction of solid and the composition of the new liquidus at each point. Susceptible alloys have large solidification ranges between the liquidus and solidus temperatures and sharp turnover in the solidification curves at high fractions of solid [42]. The sharp turnover is typically associated with the increased levels of strengthening solute that partitions in the liquid to a high degree during solidification. Associated thermal shrinkage leads to tearing and cavitation in that thin films of interdendritic liquid that is present at the high solid fraction.

Decreasing the solid fraction at which the turnover occurs or reducing the difference between the solidus and liquidus temperatures will improve resistance to tearing. Clearly, the Al-5Mg_2Si-2Mg alloy has a turnover at lower solid fraction and the difference between liquidus and solidus temperature is at a level of 31 ^oC, leading to a low tendency for cracking during solidification. The fraction of solid phase evolved during solidification with lowering the temperature calculated using Scheil-Gulliver non-equilibrium solidification model.

Meanwhile, due to the narrow solidification range by adding extra Mg into the pseudo-binary Al-Mg_2Si alloys still exhibit a typical hypoeutectic microstructure. The morphology and the size of eutectic Mg_2Si have a great influence on the mechanical properties of the materials. It is highly desirable to be able to limit the growth of Mg_2Si phase under high cooling rate during solidification. SLM processing can offer rapid solidification at a cooling rate, which is an effective way to modify the Al/Mg_2Si eutectic. Therefore, the morphology of Mg_2Si can be maintained compact and the size is well refined.

4.2. Strengthening and mechanical properties

Al-5Mg_2Si-2Mg alloy fabricated by SLM in this study exhibits a high yield strength of 295 MPa. The alloys are normally strengthened by various strengthening mechanisms mainly including solid solution hardening; grain refinement, secondary phase strengthening and Orowan strengthening mechanism.

In the alloy, Mg_2Si can potentially maximize the solid solution strengthening. The lattice parameter of Mg_2Si (6.35 Å × 6.35 Å ×6.35 Å) is larger than Al (4.05 Å × 4.05 Å ×4.05 Å). It is known that rapid cooling during solidification can lead to a significant increase in the solid solubility. According to the equilibrium phase diagram in Figure 11a, the effect of solid solution strengthening comes from the solute Mg and Mg_2Si in Al matrix. During the SLM forming process, the rapid cooling in the molten pool hinders the formation of Mg_2Si particles, resulting in supersaturation of Mg_2Si in the Al matrix. These enhance the solid-solution strengthening to improve the strength of Al-5Mg_2Si-2Mg alloy processed by SLM.

Also, the strengthening by grain refinement is significant as the results of the combination of heterogeneous nucleation and growth restriction of SLM process. This benefits from the formation of fine equiaxed grains [43,44]. The strengthening from grain size is well known according to Hall-Patch model.

The *in-situ* eutectic Mg_2Si particles are located at the grain boundaries, as shown in Figure 9. Large amounts of nanoscale Mg_2Si particles segregated at grain boundaries of Al matrix can impede the boundary sliding under stress. The pinning effect has been theoretically descripted by Zener pinning [45]. Meanwhile, nanoscale Mg_2Si particles possibly offer the effect of precipitates in the alloy, although no systematic evidence is observed. It is suspected that the fine Mg_2Si particles may also promote the dislocation bowing because of the coherency between Mg_2Si and Al matrix, which could offer the strengthening likely to be so-called Orowan mechanism. Obviously, the unique microstructures in SLM fabricated alloys may contain unique strengthening mechanisms and these need to be systematically investigated for better understanding.

5. Conclusions

In this work, the effect of SLM on the microstructure and mechanical properties of an Al-5Mg_2Si-2Mg alloy was studied. The SLM fabricated alloy samples have demonstrated excellent mechanical properties. The main conclusions can be drawn as follows:

(1) The Al-5Mg_2Si-2Mg alloy can be successfully processsed by SLM to make sound samples. The as-fabricated samples are free of hot cracking with limited other defects. The unique features of the alloy include (a) the reduced solidification range, (b) the possible inrease of the eutectic level in the microstructure, and (c) the shift of eutectic point and the maximum solutbility point of Mg_2Si in Al matrix.

(2) The as-SLM fabricated Al-5Mg_2Si-2Mg alloy offeres excellent mechanical properties, in which the ultimate tensile strength is 452±11 MPa, the yield strength is 295±14 MPa and the elongation is 9.3±2.5%. Clearly, these mechanical properties are greater than that obtained by high pressure die casting, and greater than many alloys obtained by SLM.

(3) The as-SLM fabricated samples are featured by significantly refined microstructure in the compact primary α-Al, the divorced Mg_2Si eutectic distributed at α-Al grain boundaries, and some of α-AlFeMnSi phase in association with eutectc Mg_2Si phase.

(4) The microstructure on the cross plane parallel to the base plate and along the building direction consists mostly of equiaxed grains at an average size of 20 μm

in the melt pool (MP) coarse zone and with very fine of 1 μm in the local area MP fine zone. Along the vertical direction on the cross plane perpendicular to the base plate, the morphology of columnar grains are obvious and the size can be up to hundreds of microns long and up to 1-20 μm wide.

(5) HR-TEM image for the interface of Al/Mg_2Si show that the Al cell have a good orientation with Mg_2Si in Al(001)//Mg_2Si(001). The coherent interface is possibly very important for enhancing the strengthening effect under as-fabricated condition. This could be important benefits for the alloy processed by SLM.

Acknowledgments

The financial support from the National Key Research and Development Program of China (grant number 2020YFB0311300ZL) is greatly acknowledged. Financial support from National Natural Science Foundation of China (No.52071343) is gratefully acknowledged as well. The author Hailin Yang would like to acknowledge useful discussion and suggestion with Dr. Dong Qiu from RMIT University.

References

[1] D. Buchbinder, H. Schleifenbaum, S. Heidrich, W. Meiners, J. Bültmann, High Power Selective Laser Melting (HP SLM) of Aluminum Parts. Physics Procedia 12 (2011) 271–278.

[2] J. Zhang, B. Song, Q. Wei, D. Bourell, Y. Shi, A review of selective laser melting of aluminum alloys: Processing, microstructure, property and developing trends. Journal of Materials Science & Technology 35 (2019) 270–284.

[3] E.O. Olakanmi, R.F. Cochrane, K.W. Dalgarno, A review on selective laser sintering/melting (SLS/SLM) of aluminium alloy powders: Processing, microstructure, and properties, Progress in Materials Science 74 (2015) 401–477.

[4] H. Attar, M. Bönisch, M. Calin, L.C. Zhang, S. Scudino, J. Eckert, Selective laser melting of in situ titanium–titanium boride composites: processing, microstructure and mechanical properties, Acta Mater. 76 (2014) 13–22.

[5] X. Cai, A. A. Malcolm, B. S. Wong, Z. Fan, Measurement and characterization of porosity in aluminium selective laser melting parts using X-ray CT. Virtual and Physical Prototyping, 10 (2015)195–206.

[6] S. Siddique, M. Imran, F. Walther, Very high cycle fatigue and fatigue crack

propagation behavior of selective laser melted AlSi12 alloy, International Journal of Fatigue 94 (2017) 246–254.
[7] H. Zhang, H. Zhu, T. Qi, Z. Hu, X. Zeng, Selective laser melting of high strength Al–Cu–Mg alloys: Processing, microstructure and mechanical properties, Materials Science& Engineering A656 (2016) 47–54.
[8] P. Wang, L. Deng, K.G. Prashanth, S. Pauly, J. Eckert,S. Scudino. Microstructure and mechanical properties of Al-Cu alloys fabricated by selective laser melting of powder mixtures. Journal of Alloys and Compounds 735 (2018) 2263–2266.
[9] P. Wang, H.C. Li, K.G. Prashanth, J. Eckert c, d, S. Scudino, Selective laser melting of Al-Zn-Mg-Cu: Heat treatment, microstructure and mechanical properties. Journal of Alloys and Compounds 707 (2017) 287–290.
[10] Y. Shi, K. Yang, S. K. Kairy, F. Palm, X. Wu, P. A. Rometsch, Effect of platform temperature on the porosity, microstructure and mechanical properties of an Al–Mg–Sc–Zr alloy fabricated by selective laser melting, Materials Science & Engineering A 732 (2018) 41–52.
[11] A.B. Spierings, K. Dawson, T. Heeling, P.J. Uggowitzer, R. Schäublin, F. Palme, K.Wegener, Microstructural features of Sc- and Zr-modified Al-Mg alloys processed by selective laser melting. Materials and Design 115 (2017) 52–63.
[12] W. Li, S. Li, J. Liu, A. Zhang, Y. Zhou, Q. Wei, C. Yan, Y. Shi, Effect of heat treatment on AlSi10Mg alloy fabricated by selective laser melting: Microstructure evolution, mechanical properties and fracture mechanism. Material Science Engineering A 663 (2016) 116–125.
[13] K. V. Yang, P. Rometsch, C.H.J. Davies, A. Huang, X. Wu, Effect of heat treatment on the microstructure and anisotropy in mechanical properties of A357 alloy produced by selective laser melting, Materials and Design 154 (2018) 275–290.
[14] N. Takata, H. Kodaira1, A. Suzuki, M. Kobashi, Size dependence of microstructure of AlSi10Mg alloy fabricated by selective laser melting, Materials Characterization 143 (2018) 18–26.
[15] F. Yan, S. Ji, Z. Fan, Effect of Excess Mg on the Microstructure and Mechanical Properties of Al-Mg_2Si High Pressure Die Casting Alloys, Materials Science Forum 765 (2013) 64–68.
[16] S. Ji, D. Watson, Y. Wang, M. White, Z. Fan, Effect of Ti addition on mechanical properties of high pressure die cast Al-Mg-Si alloys. Materials Science Forum 765 (2013) 23–27.
[17] S. Ji, F. Yan, Z. Fan, Development of a high strength Al–Mg_2Si–Mg–Zn based

alloy for high pressure die casting, Materials Science &E ngineering A 626 (2015) 165–174.
[18] L.N. Carter, X Wang, N Read. Process optimization of selective laser melting using energy density model for nickel based superalloys. Mater Sci Tech. 32 (2015) 1–5.
[19] K. G. Prashanth,S. Scudino,T. Maity,J. Das &J. Eckert. Is the energy density a reliable parameter for materials synthesis by selective laser melting? Materials Research Letters. 2017 VOL. 5, NO. 6, 386–390.
[20] L.C. Zhang, D. Klemm, J. Eckert, Y.L. Hao, T.B. Sercombe, Manufacture by selective laser melting and mechanical behavior of a biomedical Ti–24Nb–4Zr–8Sn alloy, Scripta Materialia. 65 (2011) 21–24.
[21] Y.J. Liu, Z. Liu, Y. Jiang, G.W. Wang, Y. Yang, L.C. Zhang, Gradient in microstructure and mechanical property of selective laser melted AlSi10Mg, Journal of Alloys and Compounds 735 (2018) 1414–1421.
[22] J.C. Wang, Y.J. Liu, C.D. Rabadia, S.X. Liang, T.B. Sercombe, L.C. Zhang, Microstructural homogeneity and mechanical behavior of a selective laser melted Ti-35Nb alloy produced from an elemental powder mixture, Journal of Materials Science & Technology, 61 (2021) 221–233.
[23] S. Ji, W. Yang, F. Gao, D. Watson, Z. Fan, Effect of iron on the microstructure and mechanical property of Al–Mg–Si–Mn and Al–Mg–Si diecast alloys, Materials Science and Engineering A 564 (2013) 130-139.
[24] T. Kimura, T. Nakamoto, Microstructures and mechanical properties of A356 (AlSi7Mg0.3) aluminum alloy fabricated by selective laser melting. Materials and Design 89 (2016) 1294–1301.
[25] J.H. Rao, Y. Zhang, K. Zhang, X. Wu, A. Huang, Selective laser melted Al-7Si-0.6Mg alloy with in-situ precipitation via platform heating for residual strain removal. Materials & Design 182 (2019) 108005.
[26] M. Fousova, D. Dvorsky, M. Vronka, D. Vojtech, P. Lejcek, The use of selective laser melting to increase the performance of AlSi9Cu3Fe alloy, Materials (Basel) 11 (2018) 1918.
[27]https://www.slm-solutions.com/fileadmin/user_upload/MDS_AL-Alloy_AISICu3_021 9.pdf.
[28] N. Read, W. Wang, K. Essa, M.M. Attallah, Selective laser melting of AlSi10Mg alloy: Process optimisation and mechanical properties development. Materials and Design 65 (2015) 417–424.

[29] K. Kempen, L. Thijs, J.V. Humbeeck, J.P. Kruth, Processing AlSi10Mg by selective laser melting: parameter optimisation and material characterization. Material Science Technology 31 (2015) 917–923.
[30] P. Wei, Z. Wei, Z. Chen, J. Du, Y. He, J. Li, Y. Zhou, The AlSi10Mg samples produced by selective laser melting: single track, densification, microstructure and mechanical behavior. Appllied Surface Science 408 (2017) 38–50.
[31] N.T. Aboulkhair, I. Maskery, C. Tuck, I. Ashcroft, N.M. Everitt, The microstructure and mechanical properties of selectively laser melted AlSi10Mg: The effect of a conventional T6-like heat treatment. Material Science Engineering A 667 (2016) 139–146.
[32] M. Fousová, D. Dvorsky, A. Michalcová, D. Vojtech, Changes in the microstructure and mechanical properties of additively manufactured AlSi10Mg alloy after exposure to elevated temperatures. Materials Characterisation 137 (2018) 119–126.
[33] I. Rosenthal, A. Stern, N. Frage, Strain rate sensitivity and fracture mechanism of AlSi10Mg parts produced by selective laser melting, Material Science Engineering A 682 (2017) 509–517.
[34] L. Hitzler, C. Janousch, J. Schanz, M. Merkel, B. Heine, F. Mack, W. Hall, A. Öchsner, Direction and location dependency of selective laser melted AlSi10Mg specimens, Journal Material Process. Technol. 243 (2017) 48–61.
[35] A.V. Pozdniakov, A. Yu. Churyumov, I.S. Loginova, D.K. Daubarayte, D.K. Ryabov, V.A. Korolev. Microstructure and properties of novel AlSi11CuMn alloy manufactured by selective laser melting. Materials Letters 225 (2018) 33–36.
[36] X. Li, X. Wang, M. Saunders, A. Suvorova, L. Zhang, Y. Liu, M. Fang, Z. Huang, T.B. Sercombe, A selective laser melting and solution heat treatment refined Al-12Si alloy with a controllable ultrafine eutectic microstructure and 25% tensile ductility. Acta Materialia 95 (2015) 74-82.
[37] K.G. Prashanth, S. Scudino, H.J. Klauss, K.B. Surreddi, L. Löber, Z. Wang, A.K. Chaubey, U. Kühn, J. Eckert, Microstructure and mechanical properties of Al–12Si produced by selective laser melting: Effect of heat treatment. Material Science Engineering A 590 (2014) 153–160.
[38] Y. Bai, Y. Yang, Z. Xiao, M. Zhang, D. Wang, Process optimization and mechanical property evolution of AlSiMg0.75 by selective laser melting. Materials and Design 140 (2018) 257–266.
[39] M. A. Easton, M. A. Gibson, S. Zhu and T. B. Abbott, An a priori hot-tearing

indicator applied to die-cast magnesium-rare earth alloys, Metallurgical and Materials Transactions A, 45A(2014) 3586-3595.
[40] S. Kou, A simple index for predicting the susceptibility to solidification cracking, Welding Journal, 94(2015)374-388.
[41] S. Kou, A criterion for cracking during solidification, Acta Materialia, 88(2015) 366-374.
[42] F. Liu, X.Zh. Zhu, S. Ji, Effects of Ni on the microstructure, hot tear and mechanical properties of Al–Zn–Mg–Cu alloys under as-cast condition, Journal of Alloys and Compounds, 821 (2020) 153458.
[43] X.P. Li, G. Ji, Z. Chen, A. Addad, Y. Wu, H.W. Wang, J. Vleugel, J.V. Humbeeck, J.P. Kruth, Selective laser melting of nano-TiB2 decorated AlSi10Mg alloy with high fracture strength and ductility, Acta Mater. 129 (2017) 183−193.
[44] Q.Y. Tan, J.Q. Zhang, Q. Sun, Z.Q. Fan, G. Li, Y.Yin, Y.G. Liu, M.X. Zhang, Inoculation treatment of an additively manufactured 2024 aluminium alloy with titanium nanoparticles, Acta Mater. 129 (2017) 1−16.
[45] N. Moelans, B. Blanpain, P. Wollants, Pinning effect of second-phase particles on grain growth in polycrystalline films studied by 3-D phase field simulations [J]. Acta Mater. 55 (2007) 2173−2182.